Available online at www.sciencedirect.com
SCIENCE DIRECT®
Journal of Membrane Science 239 (2004) 65–79
journal of MEMBRANE SCIENCE
www.elsevier.com/locate/memsci

Separation of dilute electrolytes in poly(amino acid) functionalized microporous membranes: model evaluation and experimental results

Aaron M. Hollman [a], Noah T. Scherrer [a], A. Cammers-Goodwin [b], D. Bhattacharyya [a,*]

[a] *Department of Chemical and Materials Engineering, University of Kentucky, Lexington, KY 40506-0046, USA*
[b] *Department of Chemistry, University of Kentucky, Lexington, KY 40506, USA*

Received 4 March 2003; received in revised form 2 July 2003; accepted 18 July 2003

Available online 15 April 2004

Abstract

Pressure-driven transport of dilute electrolytes in microporous membranes containing terminally-anchored charged poly(amino acids) (PAA) has been investigated through both experimental characterization and model evaluation. The membrane pore structure was modified via single-point covalent attachment of either negatively (poly(L-glutamic acid) or PLGA) or positively-charged polypeptides (poly(L-arginine) or PLA and poly(L-lysine) or PLL) allowing for separations using microporous materials (i.e. cellulosic, silica/polyethylene composites). Thus, efficient exclusion of ionic species can be achieved in open membrane platforms with considerably lower pressure requirements than conventional NF. For instance, the solute rejection of 0.5 mM solutions of environmentally-toxic species, such as divalent oxyanions of As(V) and Cr(VI), using a PLGA functionalized silica support (pore size ~100 nm) was >80% at 0.7 bar. The effects of solute type, concentration, pH, polypeptide loading and pore coverage of the attached macromolecule on the observed solute rejection and hydraulic permeability have been examined. In addition, immobilization of PLGA allows for conformation-based alteration of membrane separation properties upon changes in pH. These morphological transitions were investigated through application of permeability data to a two-region pore model describing solvent transport. This allows for theoretical evaluation of the effective thickness of the polypeptide-containing pore region. Ion transport was then modeled using a two-dimensional approach based on the extended-Nernst Planck equations coupled with Donnan equilibrium principles. The required parameters are the effective membrane surface charge density and the PAA pore coverage as determined through permeability studies. This analysis allows for evaluation of the fixed membrane charge density based on solute rejection data, as well as, estimation of the electrostatic properties of the immobilized poly(amino acids) (i.e. pK_a shifts, pH dependent thickness of polymer containing pore region).

Keywords: Polypeptide; Nanofiltration; Poisson–Boltzmann; Immobilization; Ion selectivity; Helix-coil; Water treatment; Charge density; As(V); Cr(VI)

1. Introduction

The development of novel membrane architectures can be accomplished by the alteration of base polymer or inorganic substrate properties or through the surface modification of existing materials via chemical treatment. The latter approach allows for the tailoring of specific properties (i.e. selectivity, resistance to biofouling, reaction kinetics) using support materials with well-established characteristics (i.e. mechanical or thermal stability). Of the various surface modification techniques, the immobilization of functional macromolecules within microporous media has gained interest due to possible applications involving chiral recognition [1], photo-modulated sensor design [2], high capacity ion-exchange [3–5] and tunable membrane separations [6]. The primary objective of this study is to investigate the applicability of poly(amino acid) (PAA) functionalized microporous membranes to the separation of dilute electrolytes (such as, As(V), Cr(III), Cr(VI)) from aqueous solutions. In addition, theoretical evaluation of ion transport in these functionalized porous materials will be analyzed using a two-dimensional model based on the extended Nernst–Planck equations coupled with Donnan equilibrium principles.

Increasingly stringent government regulation regarding the maximum contaminant level (MCL) of toxic metals in groundwater, such as arsenic (MCL = 10 μg/l) and

Abbreviations: BC, bacterial cellulose; GOPS, 3-glycidoxypropyltrimethoxysilane; PAA, poly(amino acid); PE, polyethylene; PLGA, poly(L-glutamic acid); PLA, poly(L-arginine); PLL, poly(L-lysine); PVP, poly(vinylpyrrolidone)

* Corresponding author. Tel.: +1-859-257-2794; fax: +1-859-323-1929.
E-mail address: db@engr.uky.edu (D. Bhattacharyya).

0376-7388/$ – see front matter © 2004 Elsevier B.V. All rights reserved.
doi:10.1016/j.memsci.2003.07.026

chromium (MCL = 50 μg/l), has facilitated a need for separation processes designed specifically for dilute systems. Inorganic arsenic and chromium, both known carcinogens, are typically present in surface and groundwater as divalent oxyanions ($HAsO_4^{2-}$, CrO_4^{2-} or $Cr_2O_7^{2-}$) making them ideal solutes for charged-based membrane separations. Nanofiltration (NF) has been recognized as a promising sustainable technology for removal of these toxic compounds. However, NF processes require applied pressures of around 10 bar to achieve adequate separation. The range of applicability of charged membrane processes for the separation of ionic solutes would increase significantly with the development of platforms with reduced pressure requirements (<5 bar) and thus greater energy efficiency.

In this study, high molecular weight charged polypeptides (poly(L-glutamic acid) or PLGA, poly(L-arginine) or PLA and poly(L-lysine) or PLL) have been incorporated within the pore structure of both silica and cellulose-based microporous (0.1–0.2 μm) supports through single-point covalent attachment. The long-range character of electrostatic interactions induced by these charged macromolecules not only mimics the separation mechanism of conventional NF leading to Donnan-type exclusion of ionic species, but also allows for conformation-based alteration of membrane transport characteristics (i.e. permeability, solute rejection). Ion selectivity is determined by the acidic (negatively charged, i.e. PLGA) or basic (positively charged, i.e. PLA, PLL) properties of the side groups associated with each PAA sequence. Due to the open pore geometry associated with these materials, there is much less resistance to solvent transport allowing for low-pressure operation. Grafting terminally anchored linear polymer chains avoids the need for a cross-linked polymer network. Chemical cross-linking restricts polymer chain mobility resulting in membrane materials characterized by much lower water permeability [7]. This work will establish the effects of solute type, salt concentration, pH, polypeptide loading and pore coverage of the attached macromolecule on the observed solute rejection and hydraulic permeability of these pore-modified membrane materials.

2. Background and theory

2.1. Properties of poly(amino acids)

Fundamental studies on the behavior of charged poly (amino acids) in homogeneous solution [8,9] and in terminally-anchored brush layers [10,11] reveals interesting properties useful for advanced material design. The morphology of charged polypeptides in homogeneous solution has been well established to depend on the properties (pH, ionic strength, counter-ion type) of its surrounding environment. These titrating polyelectrolytes are particularly well suited for modulating chemical signals because their morphology is dependent upon the electrostatic interactions between side group constituents. Due to the proximity of their titrating sites, the acidic or basic properties of poly(amino acids) can dramatically differ from their corresponding monomeric residues. The average degree of ionization, α, of a polyacid chain (i.e. PLGA) is related to its dissociation constant, K_a, according to the active mass law

$$\frac{\alpha}{1-\alpha} = \frac{K_a}{[H_3O^+]} \quad (1)$$

where $[H_3O^+]$ is the concentration of protons in solution. For monoacids in solution, the dissociation constant ($K_a = K_{a0}$) is a quenched property, one that is both fixed and independent of external conditions. In contrast, the dissociation constant associated with charged macromolecules varies with its degree of ionization. Electrostatic interactions between neighboring charged side chains of polyacids adversely affect the overall tendency of the macromolecule to deprotonate. Thus, increasing values of α are accompanied by a subsequent change in the apparent dissociation constant ($\Delta pK_a = pK_a - pK_{a0}$) [12]. The magnitude of the pK_a shift can also depend upon the morphology of the polymer chain, in particular, the spacing between its adjacent titrating sites. Conformational transitions, well documented for polypeptides in solution, mitigate the effects of intramolecular charge interactions resulting in a lowering of ΔpK_a.

Immobilization, whether covalent or non-covalent, can also introduce significant differences in the characteristics of charged poly(amino acids). Abe et al. [13] studied the intermolecular interactions between opposed brush layers of grafted PLGA through surface force measurements. This research group determined that the electrostatic behavior of the immobilized polypeptide was dependent upon the density of the grafted polymer chains. Above a critical density of about 0.2 chains/nm^2 [13], counterions become tightly bound to the macromolecule suppressing its degree of ionization. This suggests that the optimal utilization of the attached polyelectrolytes with regards to ion-selective separations will be at values below this critical density. Sufficient chain spacing should allow the immobilized macromolecule to exhibit the diffuse electrostatic behavior that has been observed in the solution phase.

2.2. Model considerations

The separation behavior of these PAA functionalized membranes was modeled assuming a cylindrical pore geometry with polypeptide chains uniformly bound along the pore wall. At this point, the effects of pore size distribution and irregular pore geometry on solute retention were ignored for simplicity. This idealized pore, shown in Fig. 1, suggests two distinctly different regions of ionic transport. The properties (size, electric potential) of each region of the pore cross-section are dependent upon the chemical nature of the contacting solution (pH) and will be modeled accordingly.

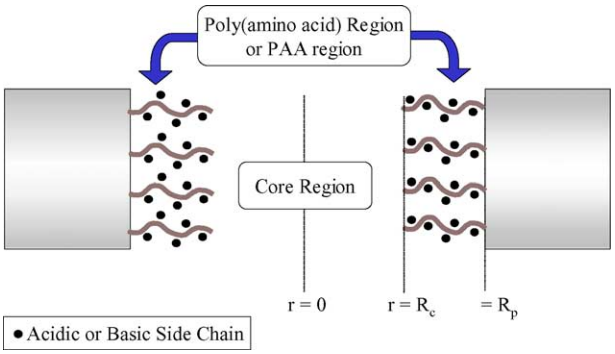

Fig. 1. Schematic representation of a model cylindrical membrane pore containing terminally bonded charged poly(amino acids).

2.2.1. Two-region velocity profiles

The conformational (i.e. helix, random coil) transitions of the grafted polypeptide require the use of a moving interface (pH dependent) between the core and PAA regions (see Fig. 1). In other words, the position of the boundary ($r = R_c$) separating the two regions varies with pH. This radial dependence can be approximated through permeate flux measurements at varying solution pH. In the region devoid of the grafted macromolecules ($0 \leq r < R_c$), termed the core region, the velocity distribution in the radial direction, $u^c(r)$, is described by the equation of motion,

$$\frac{1}{r}\frac{d}{dr}\left(r\frac{du^c}{dr}\right) + \frac{1}{\mu}\frac{dP}{dx} = 0 \tag{2}$$

where x is the axial variable of the capillary, P is the hydraulic pressure and μ is the dynamic viscosity. Solvent transport through the semi-permeable PAA region ($R_c < r \leq R_p$) can be determined using the well known Debye–Brinkman equation,

$$\frac{1}{r}\frac{d}{dr}\left(r\frac{du^B}{dr}\right) - \frac{u^B}{\kappa} + \frac{1}{\mu}\frac{dP}{dx} = 0 \tag{3}$$

where $u^B(r)$ is the PAA region velocity profile and κ is the solvent-specific hydraulic permeability coefficient associated with this polypeptide containing region [14]. The coupled velocity distribution, $u(r)$, was solved through simultaneous evaluation of Eqs. (2) and (3) subject to the boundary conditions,

$$\begin{aligned} &u^B(R_p) = 0, \qquad \frac{du^c}{dr}(0) = 0 \\ &u^c(R_c) = u^B(R_c), \quad \frac{du^B}{dr}(R_c) = \frac{du^c}{dr}(R_c) \end{aligned} \tag{4}$$

where R_c represents the solution-dependent radial boundary between the core and PAA region. The permeability coefficient (κ) and the dependence of R_c on pH were determined through an iterative procedure involving the integration of the predicted velocity profiles over the pore cross-sectional area,

$$J_{v,p} = \frac{J_v}{(\varepsilon/\tau)} = \frac{\int_0^{R_c} u^c(r)r\,dr + \int_{R_c}^{R_p} u^B(r)r\,dr}{\int_0^{R_p} r\,dr} \tag{5}$$

where $J_{v,p}$ is the solvent flux within the membrane pore, J_v is the experimentally measured solvent flux and (ε/τ) is the ratio of membrane porosity to tortuosity. The permeability coefficient (κ) was adjusted until the calculated solvent flux was in close agreement with corresponding experimental measurements. Cohen et al. used this two-region pore flow approach to describe shear-induced permeability changes (i.e. the effect of solvent shear on chain orientation) in porous membranes functionalized with poly(vinylpyrrolidone) (PVP) [14]. In contrast, the current study uses this modeling procedure to quantify changes in the effective hydrodynamic thickness associated with the morphological transitions of terminally grafted biomolecules.

2.2.2. Equilibrium partitioning

The rejection of single salt solutions by charged membranes is greatly influenced by the equilibrium distribution of co-ions (ions with same charge as the membrane bound functional groups) at the membrane–solution interface. Due to this ion-partitioning effect, a potential difference (i.e. the Donnan potential) is induced to maintain electrochemical equilibrium. Given the conditions of electroneutrality in the membrane and solution phases, the co-ion distribution for a negatively charged membrane in contact with a dilute single salt solution is described by

$$\frac{c_2^m}{c_2} = \left[\frac{|z_2|c_2}{|z_2|c_2^m + |z_x|Q}\right]^{|z_2|/|z_1|} \tag{6}$$

where z_i is the ion valency (1, cation; 2, anion) and z_x is the valency associated with the fixed membrane charge, Q (superscript 'm' denotes membrane phase) [15]. For membranes grafted with charged poly(amino acids), Q is dependent upon the degree of grafting, polypeptide chain length (degree of polymerization) and the solution pH (see Eq. (1)). It should be noted that for these experiments, the starting counterions for anionic PLGA was Na^+ and for cationic PLA and PLL was Cl^-.

2.2.3. Two-dimensional ion transport

Modeling ion transport in charged media has been a fundamental aspect of membrane science since the mid-sixties with the classic works of Kedem and coworkers [16,17]. In relatively dense charged membranes (pore <3 nm), ion transport is generally well described through a one-dimensional approach that assumes a uniform distribution of electric potential and solute concentration in the radial direction [18,19]. However, this assumption is not valid for membranes with much larger pore dimensions. For two-dimensional ion transport at steady state, the flux of ion i in the axial ($j_{x,i}$) and radial ($j_{r,i}$) direction can be described using the extended Nernst–Planck equations,

$$j_{r,i} = u(r)c_i^m - D_i\left(\frac{\partial c_i^m}{\partial r} + \frac{z_i c_i^m F}{RT}\frac{\partial \Phi}{\partial x}\right) \tag{7}$$

$$j_{r,i} = -D_i \left(\frac{\partial c_i^m}{\partial r} + \frac{z_i c_i^m F}{RT} \frac{\partial \Phi}{\partial r} \right) \quad (8)$$

where D_i is the ion diffusivity in the membrane phase, R is the gas constant, F is the Faraday constant, T is the absolute temperature and Φ is the total electric potential. To account for the radial distribution in the electric potential, Gross and Osterle first proposed to represent Φ as the superposition of two distinct entities

$$\Phi(x, r) = \psi(x, r) + \varphi(x) \cong \psi(r) + \varphi(x) \quad (9)$$

where ψ is the double layer potential originating from the membrane charge and φ is the axial streaming potential [19]. Given the pore dimensions of the membranes used in this work (pore diameter: 100–200 nm), the axial variation in ψ was assumed small compared to the radial variation and both the axial and radial ion diffusivity were assumed equivalent to the bulk diffusivity of the respective ion. Substitution of Eq. (9) into Eq. (8) with the condition of negligible flux in the radial direction leads to the Boltzmann distribution,

$$c_i^m(x, r) = C_i^m(x) \exp\left(-\frac{z_i F \psi(r)}{RT} \right) \quad (10)$$

where $C_i^m(x)$ is the centerline ion concentration [20].

Given that the length of the pore is large compared to the pore radius, R_p, the Poisson equation governing the double layer potential distribution can be expressed as

$$\nabla^2 \psi(r) = -\frac{F}{\epsilon}[z_1 c_1^m(x, r) + z_2 c_2^m(x, r)] \quad (11)$$

where ϵ is the dielectric permittivity of the single salt solution [20]. The boundary conditions used to solve Eq. (11) were

$$\psi(R_c) = 0, \qquad \frac{\partial \psi}{\partial r}(R_p) = \frac{q_w}{\epsilon} \quad (12)$$

where q_w is the charge density based on the surface of the capillary [21]. The first condition requires the assumption that the double layer potential established by the grafted poly(amino acids) extends only to the core–PAA region interface ($r = R_c$). Thus in the core region, the double layer potential was assumed negligible. The second boundary condition in Eq. (12) assumes that the electric potential established by the delocalized charged side-chains of the grafted polypeptide can be approximated using a uniform surface charge density parameter. This parameter, q_w, is related to the fixed membrane charge, Q,

$$Q = \frac{2 q_w}{F R_p} \quad (13)$$

using the pore radius [22]. Therefore, evaluation of the separation performance of these membranes can be predicted using a single parameter describing the concentration of fixed charged groups within the membrane pore structure. It should be noted that the second boundary condition given in Eq. (12) is only valid for dilute solutions with constant electrical permittivity [23].

2.2.4. Model evaluation procedure

The scheme used to model solute rejection for these novel membrane platforms first required the determination of the radial position of the core–PAA region interface (R_c) as a function of solution pH as described in Section 2.2.1. Once this relationship has been established, solute rejection behavior can be calculated for a given polypeptide attachment or for a given volume density of total available ionizable groups, Q_T. This quantity is related to the fixed membrane charge, Q, by the following equation

$$Q = \alpha Q_T \quad (14)$$

using the degree of ionization of the grafted PAA chains. Therefore, the fixed membrane charge is directly associated with the pK_a of the attached polypeptide and the solution pH via Eq. (1). For the corresponding values of Q, Eq. (6) can be used to calculate the effects of ion-partitioning at both membrane–solution interfaces.

The next step in the solution algorithm was to substitute Eqs. (9) and (10) into Eq. (7) resulting in the following expression

$$j_{x,i} = \exp\left(\frac{z_i F \psi(r)}{RT} \right) \times \left[u(r) C_i^m - D_i \left(\frac{dC_i^m}{dx} + \frac{z_i C_i^m F}{RT} \frac{d\varphi}{dx} \right) \right] \quad (15)$$

for the local ion ($i = 1, 2$) flux in the axial direction. Integration of Eq. (15) over the pore cross-sectional area,

$$J_i = \frac{\int_0^{R_p} j_{i,x} r \, dr}{\int_0^{R_p} r \, dr} = \frac{2}{R_p^2} \left[K_i(C_i^m) C_i^m - L_i(C_i^m) D_i \times \left(\frac{dC_i^m}{dx} + \frac{z_i C_i^m F}{RT} \frac{d\varphi}{dx} \right) \right] \quad (16)$$

where

$$K_i(C_i^m) = \int_0^{R_p} u(r) \exp\left(-\frac{z_i F \psi(r)}{RT} \right) r \, dr,$$

$$L_i(C_i^m) = \int_0^{R_p} \exp\left(-\frac{z_i F \psi(r)}{RT} \right) r \, dr \quad (17)$$

yields a one dimensional differential equation for the overall ion flux, J_i ($i = 1, 2$) [20]. Evaluation of the integrals shown in Eq. (17) can be determined through solution of the Poisson equation (Eq. (11)) at values of the solute concentration ranging from the feed to permeate. Using the condition of no electric current,

$$\sum_i F z_i J_i = 0 \quad (18)$$

the coupled ordinary differential equations given in Eq. (16) can be solved numerically to obtain the axial profile of solute concentration, and thus, the solute rejection. The aim of the proposed model is to describe electrolyte transport in porous membranes containing terminally-anchored charged macromolecules. This approach allows for theoretical evaluation

of the degree of attachment (in terms of the total available ionizable groups, Q_T) based on comparison to solute rejection data. In addition, it accounts for the dynamic behavior of the grafted biomolecule (pore coverage, degree of ionization) in response to changes in its surrounding environment and the effect of these changes on the hydraulic permeability and separation behavior of the support material.

3. Experimental

3.1. Materials

Two types of microporous supports were used in this study: a silica-based membrane (Daramic Corp.) and an aldehyde-rich support comprised of high aspect ratio bacterial cellulose (BC) fibers. The former is commercially prepared via extrusion of submicron silica particles with polyethylene resin and plasticizer. The resulting membrane contains approximately 70% silica by weight. Its pore structure is defined by the gaps between adjacent silica particles. Preparation of the aldehyde-rich cellulosic membranes is given in detail in a previous publication [6]. The silane used, 3-glycidoxypropyltrimethoxysilane (GOPS), was supplied by Aldrich. Amine-terminated poly(L-glutamic acid) (Na form, degree of polymerization $n = 241$, 356), PLA (hydrochloride, $n = 44$, 248, 270) and PLL (hydrochloride, $n = 97$, 461) were obtained from Sigma. All metal salts used unless otherwise noted were reagent grade and supplied by Fisher Scientific. Dextran with an average molecular weight of 144 kDa was also obtained from Aldrich. All aqueous feed solutions used in this study were prepared with deionized ultrafiltered water from Fisher Scientific.

3.2. Poly(amino acid) functionalization

Covalent attachment involving the amine terminus of poly(amino acids) requires the incorporation of reactive functionalities within the pore structure of the membrane material. The method of derivatization is dependent upon the properties of the base support. Activation of the cellulosic membranes used in this study was achieved through ozone oxidation resulting in a high degree of aldehyde functionality [6]. The silica-based membranes were derivatized under convective flow conditions via silanization using a 9% solution (v/v) of GOPS in *o*-xylene at room temperature. Chemical reaction between the silanol groups present within the membrane and the methoxy groups of GOPS results in epoxide formation on the pore surface. Residual silane was subsequently removed through ethanol permeation.

For both types of membrane supports, the single-point immobilization of poly(amino acids) (i.e. PLGA, PLA and PLL) was carried out through permeation of 300 ml of an approximately 150 mg/l aqueous solution at pH 9.2–9.8. The pH conditions were chosen such that the terminal amine group was not protonated and would participate in the nucleophilic attack of the surface aldehyde/epoxide groups. For cellulosic membranes, it should be noted that the imine bond produced in the Schiff base reaction was subsequently reduced via treatment with $NaBH_4$ (Sigma) to enhance acid resistance. This particular treatment was not required for the silica-based membrane since the corresponding reaction (amine/epoxide) results in a stable saturated bond.

Table 1
Physical characteristics of the membrane supports prior to polypeptide immobilization

	Cellulose	Polyethylene/silica
Average pore size (nm)	100–210	96.4
Thickness (mm)	243–392	274
Internal surface area (m^2/g)	120	80
Dry mass per external surface area (mg/cm^2)	12.7	15.3

3.3. Analysis of membrane properties

Physical properties of the base membrane supports used in this study are shown in Table 1. The approximate pore size of these membranes was estimated through scanning-electron microscope images of their cross-section as shown in Fig. 2 ((a) cellulose, (b) silica–polyethylene) using the Fovea image Processing Software Package (sample size ~200 pores). Internal surface area measurements (using N_2 at 77 K) were determined in previous studies (cellulose [5], silica–PE [4]) using a Micromeritics ASAP 2000 BET surface area analyzer. The extent of PAA attachment was measured through total organic carbon measurements (TOC 5000A total organic carbon analyzer) of the feed and permeate solutions. Experimental error for TOC analysis in the range of 5–100 mg carbon/l was less than 2% for all reported values.

Ion exclusion experiments were performed using a SEPA ST membrane cell provided by Osmonics. This apparatus has a membrane cross-sectional area of 13.2 cm^2 and contains a stirring device placed in close contact to the feed solution-membrane interface to minimize the effects of concentration polarization. All metal solution concentrations for both single and mixed electrolyte systems were measured with a Varian AA575 series atomic absorption spectrophotometer. Neutral solute rejection studies involving high-molecular weight dextran were analyzed through TOC measurements. Material balance calculations, performed on all experiments, showed <5% error verifying the separation mechanism (ion exclusion rather than adsorption).

4. Results and discussion

The low-pressure separation of electrolytes (both inorganic and organic) from dilute solutions was achieved using microporous membrane materials functionalized with charged poly(amino acids). For this particular application,

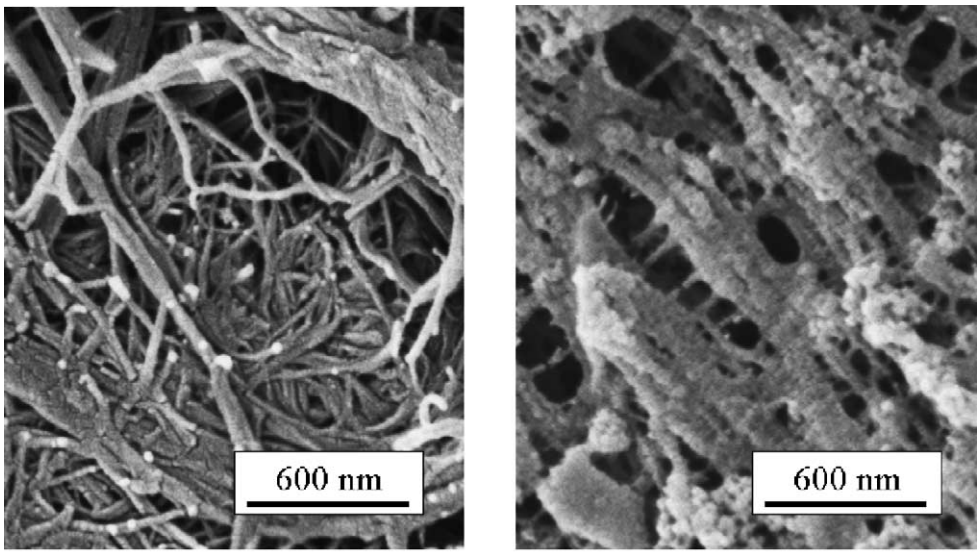

Fig. 2. SEM images (both at 50 K magnification) of the surface of the (a) cellulosic (aldehyde-rich) and (b) silica-based (epoxide-rich) support membranes.

only amino acid residues having acidic (PLGA) or basic (PLA and PLL) side chain functionalities are of interest. Of the basic residues, the charge associated with the amino group of lysine is more localized than the guanidinium cation of arginine. Therefore, the electrostatic interaction of these residues with ionic species in solution is expected to differ. The isoelectric point of histidine, the only other basic amino acid residue, is approximately 7.6 making it uncharged under neutral solution conditions and thus limiting its application to this study.

4.1. Permeability studies

The effects of solution pH on the solvent flux (at $\Delta P = 0.7$ bar) of a silica-based microporous membrane functionalized with PLGA ($n = 356$) at different attachment densities are shown in Fig. 3. Prior to polypeptide attachment, the unmodified support had an average pure water flux of 18.3×10^{-6} m/s at the corresponding applied pressure ($\Delta P = 0.7$ bar). The observed decline in permeation rate at higher pH conditions can be attributed to the conformational transition of the attached polypeptide. In the high pH regime, the carboxylate side groups of PLGA are deprotonated. The repulsive force between neighboring constituents causes the macromolecule to extend into the pore cross-section in a random-coil formation. The presence of these extended chains mitigates solvent transport resulting in lower membrane permeability. At low pH, the degree of ionization (Eq. (1)) is reduced alleviating the intramolecular force acting on the macromolecule. Under these conditions, PLGA will exist in a more compact α-helical formation reducing the PAA region thickness (see Fig. 1) causing the solvent flux to approach that of the unmodified support. Measurements of the permeate flux shown in Fig. 3 alternated between high and low pH values to illustrate the inherent reversibility of this process.

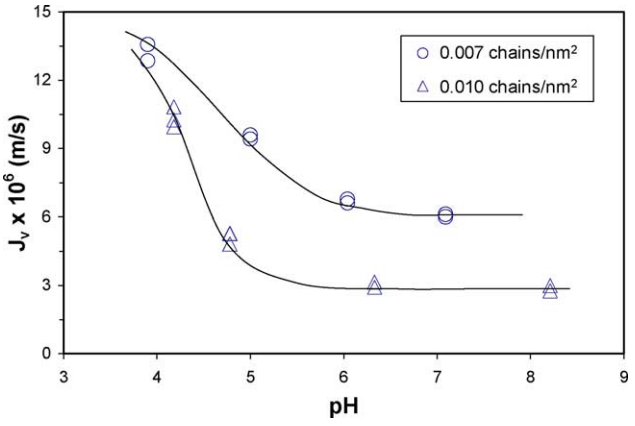

Fig. 3. Dependence of the measured solvent flux (J_v) on solution pH for a silica-based microporous membrane functionalized with poly(L-glutamic acid) ($n = 356$) at different attachment densities ($\Delta P = 0.7$ bar).

Another important aspect of Fig. 3 is the relatively low attachment density (ranging from 0.7×10^{-2} to 1.0×10^{-2} chains/nm^2) associated with these functionalized membrane materials. These values were calculated based on the internal surface area (BET surface area using N_2) determined for the unmodified silica–polyethylene composite (see Table 1). At higher attachment density (0.010 chain/nm^2), the modified support showed a much greater decline in permeate flux when compared with the lower density (0.007 chain/nm^2) support. This is obviously the result of increased steric hindrance by the attached macromolecule on solvent transport and would correspond to a lower permeability coefficient (κ) associated with the PAA region. Theoretical evaluation of κ for both membranes shown in Fig. 3 based on Eqs. (2)–(5) is given in Section 4.3.

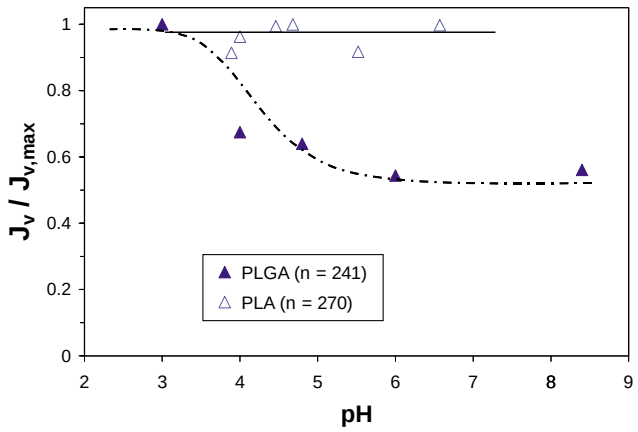

Fig. 4. Relationship between the normalized permeate flux ($J_{v,max}$ = maximum flux) and solution pH for both a poly(L-glutamic acid) [6] (PLGA, $n = 241$) and a poly(L-arginine) (PLA, $n = 270$) functionalized BC membrane.

Despite variation in the attachment density, both membranes displayed an inflection point in permeate flux at pH values in the vicinity of 4.5–5 indicating a dramatic change in the degree of ionization (α) around these values. This behavior contrasts that typically observed for materials characterized by much greater PAA attachment density. Hayashi et al. [11] measured the degree of ionization of opposed brush layers of PLGA in Langmuir–Blodgett (LB) films through FTIR spectroscopy. The LB films studied in this work had attachment densities in the vicinity of 0.4 chains/nm^2 (greater than an order of magnitude difference than the supports shown in Fig. 3). For immobilized PLGA ($n = 48$), the measured degree of ionization shifted from 0.19 at pH 9 to 0.61 at pH 10. These unusually low values of α, as well as, the high pH value of ionization transition were attributed to enhanced counterion binding to the acidic polyelectrolyte. For low attachment density (<0.2 chains/nm^2 [13]), counterions loosely bind forming a diffuse ion layer around the charged macromolecule. As the interchain distance between these molecules is reduced, counterions bind more strongly to form partially neutralized polyelectrolytes. Therefore, proper design of functionalized membrane platforms for charged-based separations must account for this transition in the binding mode of counterions at higher attachment densities.

To further verify that the dynamic behavior shown in Fig. 3 could be attributed to the conformational transitions of the grafted polypeptide, similar measurements were performed on a membrane functionalized with PLA. A comparative study between the effects of negatively-charged PLGA and positively-charged PLA on the relationship between solvent transport and solution pH is shown in Fig. 4. The results given were from separate coupons of the same fabricated BC membrane support. Flux measurements were normalized using the maximum observed permeate flux ($J_{v,max}$) for both functionalized membranes (i.e. $J_{v,max}$ (PLGA) = permeate flux at pH 3). The average degree of polymerization (n = number of repeat residues) for each grafted PAA chain was relatively similar (PLGA: $n = 241$, PLA: $n = 271$). In contrast to PLGA, membranes functionalized with PLA displayed no observed dependence between permeate flux and solution pH under the conditions used in this study (Fig. 4). The guanidinium cation (i.e. the side chain present at the α-carbon position of the amino acid residue) associated with L-arginine has a pK_a of approximately 12. Thus, PLA should remain fully ionized for the entire pH range shown in Fig. 4 and would therefore undergo no conformational transition. Conversely, monomeric L-glutamic acid has a pK_a of 4.07, indicating a definitive transition between the protonated (low pH) and ionized (high pH) state over the pH range used in Fig. 4. Estimation of the pK_a shift, ΔpK_a, from this monomeric value for terminally-grafted PLGA ($n = 356$) will be discussed in Section 4.3.

Table 2
Solute rejection of various inorganic solutes (0.5 mM, pH 8) and a neutral dextran (100 mg/l, pH 6) for a silica-based microporous membrane functionalized with poly(L-glutamic acid) ($n = 356$, 0.010 chains/nm^2) at $\Delta P = 0.7$ bar

	Solute rejection (%)
Ionic solute	
Na_2SO_4	88.6
Na_2HAsO_4 (As(V))	87.7
Na_2CrO_4 (Cr(VI))	80.0
Neutral solute	
Dextran (MW = 144 kDa)	1.5

4.2. Solute rejection studies

Experimental data regarding the solute rejection of some environmentally significant inorganic solutes (As(V), Cr(VI)) using a silica-based microporous membrane functionalized with PLGA ($n = 356$, attachment density = 0.010 chains/nm^2) is shown in Table 2. The average pore size of the host material, as determined through software analysis of SEM images (surface), was 96.4 ± 40.9 nm. Prior to polypeptide attachment, the unmodified support showed no separation of Na_2SO_4 under these same experimental conditions. Thus, the separation of ionic species can be attributed solely to the electrostatic interactions between these charged constituents and the grafted polyelectrolyte. Based on the results shown in Table 2 and the MCLs of As(V), this particular membrane would be effective treating groundwater containing ~83.1 μg/l as As(V). The results shown in Table 2 correspond to simple systems containing high levels of the contaminant; therefore, further studies would be required to establish their applicability to real systems. Differences in the retention of As(V) and Cr(VI) with respect to SO_4^{2-} could be due to partial species ionization (pK_a($HAsO_4^{2-}$) = 6.94 [24], pK_a(CrO_4^{2-}) = 6.49 [25]). At pH 8, a small percentage of these toxic metals will exist as univalent co-ions ($H_2AsO_4^-$ or $HCrO_4^-$) resulting in reduced interaction with the negatively charged membrane.

It should be noted that inorganic arsenic present in drinking water commonly exists in two oxidation states, both as a trivalent (As(III), H_3AsO_3) and pentavalent (As(V), $HAsO_4^{2-}$) oxyanion. Fortunately, pentavalent arsenic is more thermodynamically stable in oxic water and predominates in surface waters at near neutral pH [26]. Under these same conditions, As(III) remains as a neutral molecule. Thus, separation of arsenite via charged-based membrane processes would require a pre-oxidation of As(III) to As(V).

To further illustrate the separation mechanism of these functionalized membrane materials, neutral solute rejection studies were performed using 100 mg/l solutions of 144,000 MW dextran. Despite the size of this particular solute (molecular diameter = 20.0 nm [27]), the modified support showed negligible solute rejection (1.5%) as is depicted in Table 2. On the other hand, divalent ionic species with much smaller molecular dimensions (i.e. hydrated radii of SO_4^{2-} and CrO_4^{2-} is 0.379 and 0.375 nm, respectively [28]) showed retention values greater than 80%. Therefore, the barrier properties associated with these membranes are contingent upon charge interactions with the grafted polypeptide, rather than physical or steric interactions with the host material.

An aim of this study is to achieve efficient separation of ionic species from dilute solutions at markedly lower pressures than are generally required by traditional membrane processes. In general, NF processes operate at applied pressures of around 10 bar [24]. The single salt experiments reported in Table 2 were performed using 0.5 mM solutions at an applied pressure of 0.7 bar. The separation efficiency of NF-type membranes is markedly reduced at low applied pressure due to the increased contribution of diffusion to the overall solute flux. Through covalent attachment of charged macromolecules, these same charged-based separations of ionic species can be attained using membranes with much larger pore geometries. Thus, a possible application of PAA functionalized membranes could be the low-pressure removal of toxic metals, such as As(V) and Cr(VI), from contaminated water sources. Increasingly lower standards regarding the presence of these species in drinking water mandates the development of more energy efficient processes designed specifically for the removal of these toxic compounds from dilute systems.

4.2.1. pH effects

The effects of pH on the ion exclusion of a 9000 μg/l (0.12 mM) arsenate (As(V)) solution using a silica-based support functionalized with PLGA are shown in Fig. 5. The attachment density associated with this modified support was 0.007 chains/nm^2. Flux data corresponding to this solute rejection study can be found in Fig. 3. At pH 7, the measured solute rejection of As(V) was 93.2% and the hydraulic permeability (A) of the functionalized membrane was 8.8×10^{-4} cm^3/(cm^2 s bar). A high performance NF membrane, such as NF45 by Dow-Filmtec®, has a hydraulic permeability of $\sim 1.1 \times 10^{-4}$ cm^3/(cm^2 s bar) [29]. These

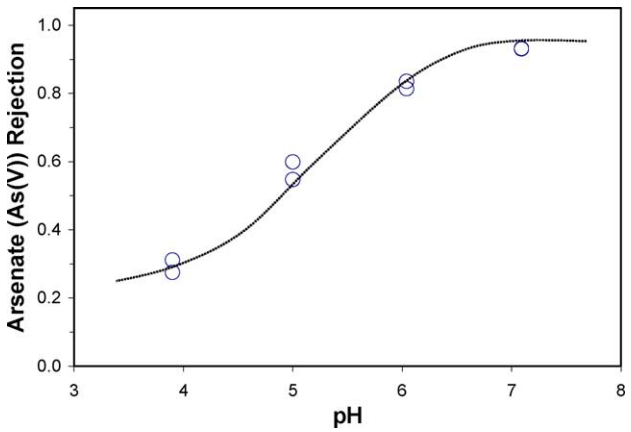

Fig. 5. Effect of feed solution pH on the ion exclusion ($\Delta P = 0.7$ bar) of a 9000 μg/l arsenate (As(V)) solution using a silica-based microporous membrane functionalized with poly(L-glutamic acid) (n = 356, 0.007 chains/nm^2).

relatively dense membrane constructs have an active layer thickness much less than 1 μm. In contrast, the microporous supports used in this study have a membrane thickness in the range of 250 μm. Thus, more significant gains in water permeability over conventional NF could be achieved using thinner host materials. The substantial decline in solute rejection, depicted in Fig. 5, at lower pH values was accompanied by a marked increase in permeate flux (see Fig. 3). This suggests that the observed decrease in solute retention is directly related to the reduced ionization of the grafted polypeptide and the subsequent increase in the core region (see Fig. 1). This coupled with the shift in As(V) species equilibrium results in a solute rejection of 29.3% and a hydraulic permeability of 19.2×10^{-4} cm^3/(cm^2 s bar) at pH 4.

This pH-dependent behavior was not observed for membranes functionalized with basic poly(amino acids) in the pH range of 3–8. The effects of solution pH on the solute rejection of both a PLGA (n = 241, 0.003 chains/nm^2) and PLA (n = 270, 0.002 chains/nm^2) functionalized cellulosic membrane are shown in Fig. 6. In general, the solute rejection achieved using BC supports was lower than corresponding experiments performed using the commercially available silica–PE composite. This is due primarily to lower polypeptide attachment densities, as well as, to slightly larger pore dimensions. The results shown in Fig. 6 are for 0.1 mM divalent co-ion (PLGA: SO_4^{2-}, PLA: Ca^{2+}) solutions at 0.4 bar. In the high pH regime, both membranes showed approximately 60% retention of the corresponding solute. At pH 4, the separation by the positively-charged PLA/BC membrane remained relatively constant, where as, the solute rejection observed for the PLGA/BC membrane dropped significantly to around 20%. These results coincide directly with the permeation studies shown in Fig. 4 and clearly indicate that the dynamic behavior of PLGA functionalized membranes is derived from the helix-coil transitions of the attached macromolecule. The stable solute rejection observed for support membranes containing immobilized PLA with regards to

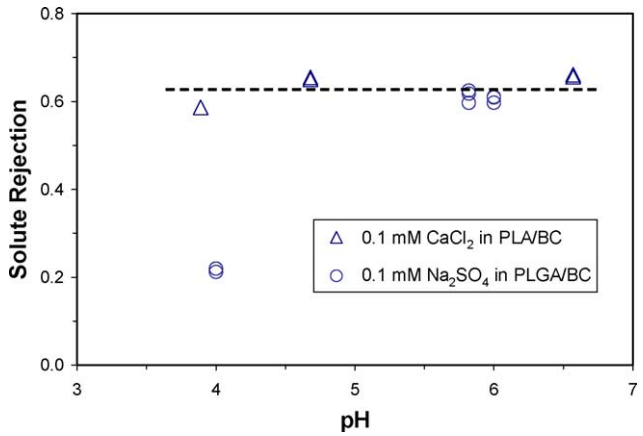

Fig. 6. Comparison between the effects of pH on the solute rejection (0.1 mM solutions, $\Delta P = 0.4$ bar) shown by both a negatively-charged poly(L-glutamic acid) (PLGA, $n = 241$, 0.003 chains/nm^2) and a positively-charged poly(L-arginine) (PLA, $n = 270$, 0.002 chains/nm^2) functionalized BC membrane.

solution pH is much more beneficial to ion separations of this type. In theory, more effective negatively-charged membranes could be developed through the terminal grafting of synthetic macromolecules with side groups consisting of sulfonic acid groups. Polymers of this type would remain ionized over broader pH ranges allowing for efficient separation of divalent anions under acidic conditions.

4.2.2. Effect of pore coverage

The inverse relationship between solute rejection and hydraulic permeability (A) for a BC membrane functionalized with positively-charged polypeptides of varying degrees of polymerization (chain length, n = number of repeat residues) is depicted in Fig. 7. These experiments were performed using 0.125 mM $CaCl_2$ solutions at $\Delta P = 1$ bar. The attachment density of the higher molecular weight PLA ($n = 270$) and PLL ($n = 461$) was 0.002 chains/nm^2. For the lower molecular weight PLA ($n = 44$), the measured attachment density was 0.005 chains/nm^2. This observed increase in attachment efficiency can be attributed to greater mobility of the polypeptide within the membrane pore and enhanced accessibility of its terminal amine group at lower molecular weight. The effects of chain length (or degree of polymerization) and reaction conditions on the attachment efficiency of poly(amino acids) using this immobilization technique is discussed in detail in a previous publication [6].

Despite the higher degree of attachment, the lower molecular weight PLA ($n = 44$) showed significantly less solute retention (~10%) than other modified supports. In addition, the hydraulic permeability associated with this support (PLA ($n = 44$)) was the highest at approximately 8.0×10^{-4} cm^3/(cm^2 s bar). Using PLA with a higher degree of polymerization ($n = 270$), the solute rejection substantially increased to around 66%. Modification with PLL ($n = 461$) showed an even further increase in rejection to approximately 94%. This clearly shows that the effectiveness of this modified membrane architecture is greatly influenced by the extension of the membrane charge into the inner portion of the pore cross-section. Proper pore coverage alleviates the effects of solute leakage in regions devoid of the charged macromolecules. However, higher pore coverage (expansion of the semipermeable PAA region (see Fig. 1)) reduces solvent transport causing a decrease in membrane permeability.

4.2.3. Effect of solute leakage

The dependence of multi-valent solute rejection on permeate flux for a silica-based microporous membrane functionalized with PLA ($n = 248$) is shown in Fig. 8. Selectivity of trivalent Cr(III) over Ca^{2+} is consistent with Donnan exclusion theory for positively-charged membranes with similar counterions (Cl^-). However, the observed decline in rejection at higher flux, particularly for Ca^{2+}, is in direct contrast to experimental trends generally observed

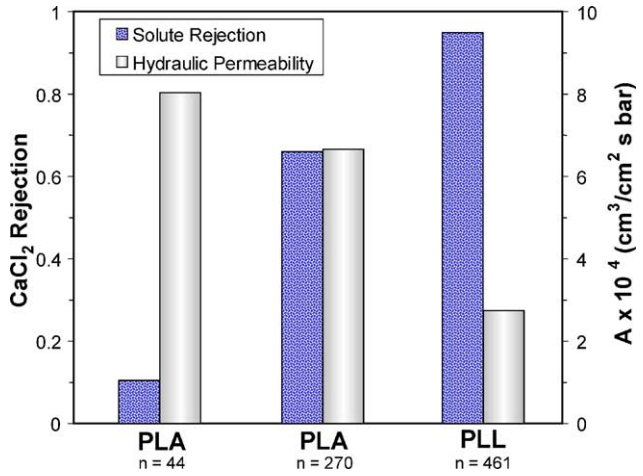

Fig. 7. Relationship between the hydraulic permeability (A) and the solute rejection ($\Delta P = 1$ bar) of 0.125 mM $CaCl_2$ solutions (pH ~ 6) for cellulosic membranes functionalized with poly(L-arginine) (PLA) and poly(L-lysine) (PLL) (n = number of repeat units).

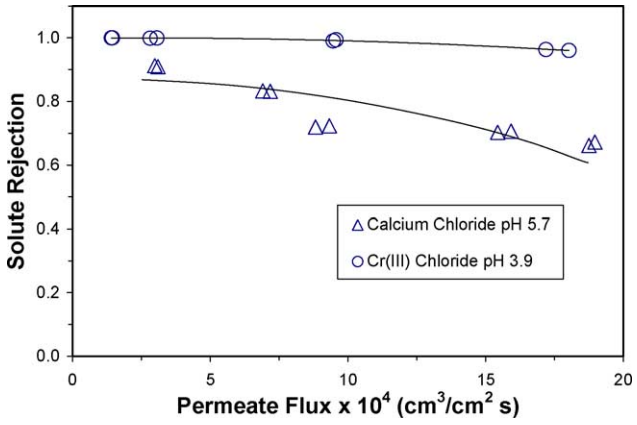

Fig. 8. The relationship between permeate flux and solute rejection of $CaCl_2$ (0.125 mM) and $CrCl_3$ (0.125 mM) for a silica-based microporous membrane functionalized with positively-charged poly(L-arginine) (PLA, $n = 248$).

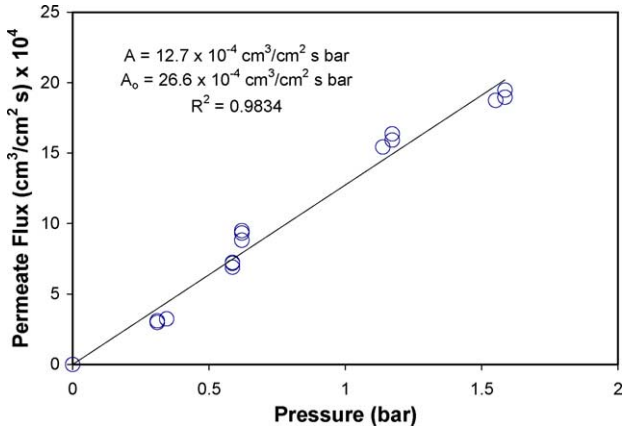

Fig. 9. The linear dependence between permeate flux and applied pressure for a silica-based microporous membrane functionalized with positively-charged poly(L-arginine) (PLA, $n = 248$).

for ion separations in dense media (i.e. reverse osmosis, NF). For NF type membranes, solute rejection increases to asymptotic values with increasing flux due to the reduced effects of diffusion at higher Peclet numbers. Sustained ion exclusion is enabled due to a relatively-constant established electric potential over the pore cross-section for membranes with nanometer dimensions. On the other hand, the microporous membranes used in this study are characterized by a non-uniform distribution of fixed charged groups within the pore geometry. This is due primarily to incomplete pore coverage by the attached polypeptide resulting from either non-uniform loading, chain orientation effects or to a low chain length to pore radius ratio. Also, the presence of small pores that restrict polypeptide attachment due to steric constraints contribute to this non-uniform distribution of charge. At higher applied pressures, there is enhanced flow through these regions of limited attachment resulting in decreased solute retention. As shown in Fig. 8, the decline in rejection was more pronounced for solutes having lower co-ion valency. The strong electrostatic interaction between the membrane and higher valency co-ions, such as Cr(III), mitigates these solute leakage effects in regions of low attachment density. Flow-induced effects, such as shear deformation of the terminally anchored polymer chains, can be assumed minimal given the linear dependence of permeate flux with applied pressure as is shown in Fig. 9. Reduction in the hydrodynamic thickness of the PAA layer ($R_c < r \leq R_p$) at higher permeate flux would perhaps be much more substantial for supports with higher chain density or at applied pressures beyond those used in this study.

4.2.4. Mixed electrolyte study (effect of valency and feed concentration)

Mixed electrolyte studies ($\Delta P = 0.3$ bar) using a ternary ($CrCl_3$, $CaCl_2$, NaCl) system of ionic species were performed on a silica-based membrane functionalized with PLA ($n = 248$). Results of these multicomponent separations at increasing feed concentration are shown in Table 3. Feed

Table 3
Solute rejection ($\Delta P = 0.3$ bar) vs. solute concentration for a silica-based microporous membrane functionalized with positively-charged poly(L-arginine) (PLA, $n = 248$) using 1:1:1 mixed electrolyte ($CrCl_3$:$CaCl_2$:NaCl) solutions (pH 3.5)

Cation	Solute rejection (%)		
	0.125 mM each (1:1:1)	0.25 mM each (1:1:1)	0.5 mM each (1:1:1)
Cr^{3+}	94.9	85.7	69.1
Ca^{2+}	93.9	81.9	61.3
Na^{+}	68.0	39.6	25.9

solutions contained equimolar (1:1:1) amounts of the three corresponding co-ions (Cr^{3+}, Ca^{2+}, Na^{+}) with a common counterion (Cl^{-}) at pH 3.5 (prevents hydrolysis of Cr(III)). The concentration of each co-ion was measured accurately using AA spectroscopy and the material balance for each co-ion showed less than 2% error. For each solute, the measured solute rejection decreased at increased electrolyte concentrations. At higher ionic strength, the electric potential established by the fixed membrane charge is reduced resulting in lower solute rejection. The retention sequence for this modified membrane support ($R(Cr^{3+}) > R(Ca^{2+}) > R(Na^{+})$) is in accordance with established theory for positively-charged membranes. Transport models for mixed electrolyte solutions in dense membranes based on the thermodynamics of irreversible processes can be found in the literature [30,31]. For simplicity, the model proposed in this study will focus on transport involving single component systems.

4.3. Theoretical analysis

The membranes used in this work are characterized by pore dimensions in the range of 100–200 nm. Given the relative size of an ionic solute (~0.3–0.4 nm), ions can be treated as point charges (i.e. no size effects) and the radial distribution of the electric potential within a porous membrane can be described using the Poisson–Boltzmann equation as first proposed by Probstein et al. [20]. The model described in this work provides an extension of this general theory of ion transport to microporous media containing terminally-anchored charged polyelectrolytes. The effective membrane charge established by immobilization of these charged macromolecules was approximated using an effective surface charge density parameter, q_w. Changes in this parameter with external solution conditions, in particular pH (i.e. well established for polypeptides), were accounted for based on the active mass law (Eq. (1)). The conformational shifts (i.e. helix-coil transitions) of the attached poly(amino acids) were modeled using a two-region hydrodynamic pore flow approach accounting for variations in solvent flux with solution conditions [14]. Model calculations were restricted to the silica–polyethylene composite membrane utilizing an average pore size of 96.4 nm. The pore characteristics of this host material were more easily defined through

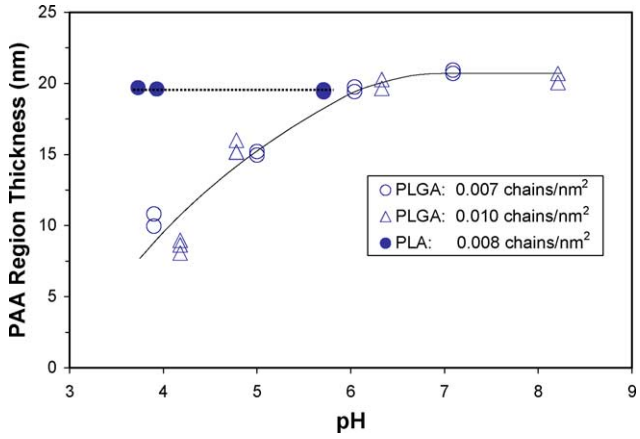

Fig. 10. Calculated dependence of the PAA region thickness ($R_p - R_c$) on solution pH based on comparison of flux data ($\Delta P = 0.7$ bar) with the proposed two-region hydrodynamic pore flow model for a microporous membrane (diameter = 96.4 nm) functionalized with PLGA ($n = 356$, open symbols) and PLA ($n = 248$, closed symbols).

software analysis of SEM images than the cellulose-based supports.

4.3.1. Determination of the hydrodynamic thickness of the brush region

The ratio of porosity to tortuosity (ε/τ) of the unmodified silica-based support was calculated using the classical Hagen–Poiseuille equation,

$$J_v = \frac{\varepsilon R_p^2}{8\mu\tau}\frac{\Delta P}{\Delta x} \quad (19)$$

where ΔP is the net applied pressure and Δx is the membrane thickness (see Table 1). Using the hydraulic permeability of the unmodified support, A_0 (shown in Fig. 9), the ratio of porosity to tortuosity (ε/τ) was determined to be 0.213. Through correction of the experimentally measured solvent flux, J_v, with this ratio, the effective thickness of the PAA region was calculated using the two-region pore flow model (Eqs. (2)–(5)). The calculated change in PAA region thickness (R_p–R_c) with solution pH for the PLGA ($n = 356$) functionalized membranes shown in Fig. 3 and the PLA ($n = 248$) functionalized membrane shown in Figs. 8 and 9 are given in Fig. 10. The thickness of the PAA region for each PLGA($n = 356$)-modified support was found to coincide at κ values of 4.0 and 0.4×10^{-17} m^2 for attachment densities of 0.007 and 0.010 chains/nm^2, respectively. Thus, it was assumed that the radial position of the boundary between the two regions was dependent solely on the degree of polymerization (n). At higher attachment, the permeability associated with the PAA region (κ) was reduced reflecting greater resistance to solvent transport. The calculated value of κ for the PLA ($n = 248$, 0.008 chains/nm^2) functionalized support was 7.5×10^{-17} m^2. Membranes containing positively-charged PLA or PLL generally showed greater hydraulic permeability than those containing negatively-charged PLGA at approximately the same conditions (chain density, number of repeat units, etc.). This is reflected in the slightly higher value of κ determined for the PLA membrane. Further experimentation is required to effectively correlate values of κ for each polypeptide with attachment density (or polymer volume fraction) as have been done for other polymer–solvent systems (i.e. PVP/water [14]). It should be noted that for real systems, the permeability coefficient κ, associated with PLGA would likely depend on pH given the conformational transitions of this titrating polyelectrolyte. For the current analysis, κ was assumed independent of solution conditions.

The results shown in Fig. 10 are in qualitative agreement with established theory for PLGA in homogeneous solutions. At pH 7, the pore coverage of the attached macromolecule was ~67.4%. Under acidic conditions (pH 3.9), this value reduced to around 33.2%, indicating a change in morphology to the more compact α-helix. The calculated PAA region thickness for the PLA ($n = 248$) functionalized membrane showed no dependence with pH under these conditions. The pore coverage associated with this PLA ($n = 248$)-silica membrane was approximately 64.7%, slightly less than PLGA ($n = 356$) at high pH.

Values corresponding to the PAA region thickness, shown in Fig. 10, do not represent the overall chain length of the attached polypeptide. Given the assumption of a model cylindrical pore with uniform attachment along the pore wall, calculations of the PAA region thickness should be viewed as an approximation of the overall pore coverage. A comparison between the values obtained in this study and those reported for a PLGA functionalized polycarbonate (PC) membrane (pore size = 200 nm) are shown in Table 4. The values reported for the PLGA/PC membrane were estimated using a Hagen–Poiseuille approach based on changes in the observed solute flux at pH values between 2 and 7 [10]. Track-etched PC membranes are characterized by well-defined pore dimensions with relatively monodisperse pore size distribution. Despite these differences in pore geometry, the values given in Table 4 for both supports show similar trends with solution pH. Changes in the PAA region thickness with pH can be attributed primarily to the enhanced intramolecular repulsive force between adjacent functionalities at higher α (i.e. at higher pH). In addition, protonation of the attached polypeptide at lower pH increases its hydropho-

Table 4
Comparison of brush region ($R_p - R_c$) calculations for the silica/PE support functionalized with PLGA ($n = 356$) to values found in the literature for a gold-coated track-etched polycarbonate membrane functionalized with PLGA ($n = 80$, 480) containing terminal thiol functionality [10]

Ito et al. (PLGA–polycarbonate) [10]			This work (PLGA–silica/PE)	
pH	PAA region thickness (nm)		pH	PAA region thickness (nm)
	$n = 80$	$n = 480$		$n = 356$
2	1.5	25	3.9	8.8
7	16	42	7	20.7

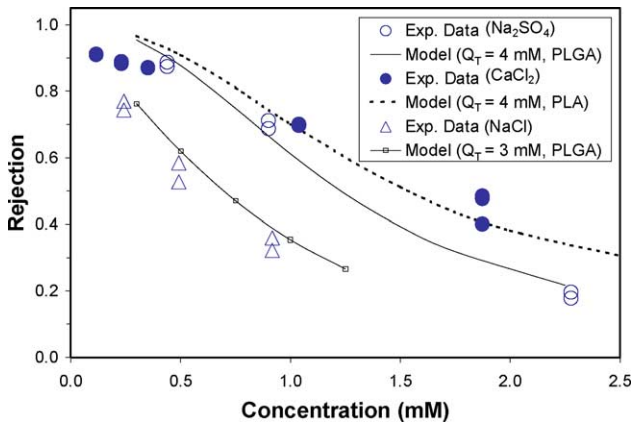

Fig. 11. Comparison of experimentally determined solute rejection ($\Delta P = 0.7$ bar) with model calculations for both a silica-based microfiltration membrane functionalized with poly(L-glutamic acid) (PLGA, $n = 356$, 0.010 chains/nm^2, pH 8) and poly(L-arginine) (PLA, $n = 248$, 0.008 chains/nm^2, pH 6).

bicity resulting in greater affinity for the host material. This would cause the macromolecule to lie on the surface of the support reducing the overall thickness of the PAA region.

4.3.2. Modeling ion transport

The model proposed in this work is based upon two input parameters: the effective membrane surface charge density (q_w) (related to Q via Eq. (13)) and the estimated pore coverage of the attached polyelectrolyte (position of R_c shown in Fig. 1). Physical properties of the host material, such as pore size and thickness, were taken as fixed values determined through membrane characterization. These properties are often used as adjustable parameters in models of ion transport in NF processes [15,18,32]. It should be noted that for the dilute concentration range used in this work, osmotic pressure effects are negligible. In addition, concentration polarization effects were negligible as verified by comparison of flux values between pure water and the electrolyte solutions.

Estimates of the PAA region thickness, shown in Fig. 10, require further model verification given that values of κ for this polymer–solvent system were not established through experimental measurement. At a specified value of κ, the relationship between pore coverage and pH can be determined through permeability measurements as described in Section 4.3.1. Using these calculated values of the PAA region thickness, the solute rejection can be determined using Eqs. (11), (12) and (16)–(18). Model calculations of solute retention should coincide with experimental measurement at the most accurate estimation of κ. Therefore, theoretical evaluation of κ in this work is an iterative process.

The dependence of solute rejection (at pH 8) on feed concentration using a silica–PE microporous support functionalized with PLGA ($n = 356$) and PLA ($n = 248$) is shown in Fig. 11. These calculations were based on values of the pore coverage shown in Fig. 10. Na_2SO_4, $CaCl_2$ and NaCl were chosen as model solutes because the valency associated with their respective ions is constant under these pH conditions. Given the pore size of the silica-based support, bulk diffusion coefficients [33] (Na^+: 1.33×10^{-9} m^2/s, Ca^{2+}: 0.79×10^{-9} m^2/s, Cl^-: 2.03×10^{-9} m^2/s, SO_4^{2-}: 1.06×10^{-9} m^2/s) were used for all model calculations.

The calculated trend in rejection with feed concentration shown in Fig. 11 is dependent upon the relationship between pore coverage and the fixed membrane charge. Overestimations of the PAA region thickness result in poor data correlation at higher feed concentrations. In the dilute concentration range, this enhanced PAA region thickness (pore coverage) will require a lower value of the calculated fixed membrane charge (Q) to correlate with the experimentally determined solute rejection. However, the saturation or shielding effect of ions on this reduced value of Q (see Eq. (6)) becomes apparent at lower feed concentration than that observed experimentally.

The model was found to best correlate with experimental data using the pore coverage values shown in Fig. 10 and at Q_T equal to 4 mM for the Na_2SO_4/PLGA system and 3 mM for NaCl/PLGA. The selection of these Q_T values gave an average relative error between calculated and experimental values of 7.7 and 11.3% for SO_4^{2-} and Cl^-, respectively. Although the values determined for Q_T using Na_2SO_4 and NaCl were similar, the fact that they were not equivalent displays the limitations of this modeling approach. A more rigorous model could incorporate the extent of uniformity of polypeptide attachment to address solute transport in regions devoid of the charged macromolecules. Therefore, an increase in the effective membrane charge would be required to account for these additional solute transport mechanisms allowing for prediction of the retention of each ion (SO_4^{2-} and Cl^-) using a single parametric value of Q_T.

As shown in Fig. 11, model calculations were also performed on a positively-charged PLA ($n = 248$, 0.008 chains/nm^2) membrane using $CaCl_2$ as a model divalent solute. The calculated value of Q_T for this $CaCl_2$/PLA system was 4 mM showing good agreement with the values determined for the PLGA functionalized membrane. For this system ($CaCl_2$/PLA), the average relative error between calculated and experimental values was 8.3%. These solute rejection experiments were performed at 0.7 bar resulting in a Peclet number (based on Ca^{2+} bulk diffusivity) of ~7.1. To provide an estimate of the contribution of diffusion to the overall solute flux, the concentration gradient term shown in Eq. (7) can be approximated via Euler's method using the membrane phase cation concentration, c_1^m, at both feed and permeate solution/membrane interfaces. For example with 0.5 mM $CaCl_2$ solutions, this approach estimates that diffusive transport contributes about 9% to the overall solute flux. Although this is a rough estimate, it is apparent that diffusion plays at least a minor role and should not be neglected in the full model assessment of ion transport in these modified membrane platforms, particularly at low pressures. The contribution of convection and electromigration to the overall solute flux is dependent upon the axial membrane position. At the pore entrance, for exam-

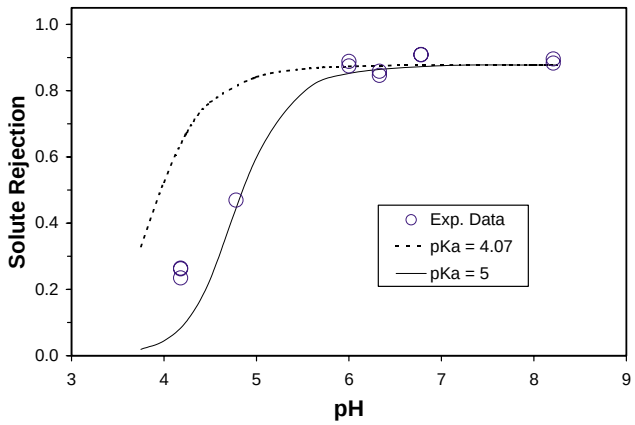

Fig. 12. Calculated pK_a shift of poly(L-glutamic acid) ($n = 356$) immobilized within a silica-based microporous membrane (diameter = 96.4 nm) using solute rejection data ($\Delta P = 0.7$ bar, 0.5 mM Na_2SO_4, $Q_T = 4$ mM).

ple, the contribution of convective transport (estimated as $J_{v,p}c_1^m(x = 0)$) for a 0.5 mM $CaCl_2$ feed solution is ~67%. The influence of convection is reduced with axial position given the corresponding decline in solute concentration. In fact, as x approaches the membrane thickness (pore exit), the role of electromigration becomes much more significant due to the inverse relationship between membrane potential and solute concentration.

4.3.2.1. Predicting shifts in the average pK_a of the attached polyelectrolyte. A unique aspect of this particular model is the ability to approximate the average shift in pK_a of the immobilized charged polyelectrolyte based on solute retention measurements at varying solution pH. The calculated pK_a shift of immobilized PLGA ($n = 356$) within a microporous silica-based support using the proposed model is shown in Fig. 12. These calculations were performed assuming an average pK_a of the attached polypeptide. Therefore, the degree of ionization (α) of the polyacid chain was modeled using Eq. (1) with an average dissociation constant, $K_{a,ave}$. The pK_a of L-glutamic acid (pK_{a0}) is approximately 4.07 [34]. As shown in Fig. 12, calculations based on this value overestimate the solute rejection in the low pH regime indicating an increase in the average dissociation constant associated with the polypeptide. Model calculations correlated best with experimental measurement using an average pK_a of 5.0 (±0.1). This shift in pK_a (Δp$K_a = 0.93$) corresponds fairly well with experimental values found in the literature for PLGA ($n = 620$, Δp$K_a = 0.51$) in dilute homogeneous solutions [35]. Therefore, the establishment of solute rejection data at varying solution pH provides a valuable tool for potentially measuring the pK_a transitions of membrane-immobilized polyelectrolytes. The observed increase in ΔpK_a for the immobilized system is perhaps due to intermolecular interactions between adjacent polypeptide chains located within this confined pore geometry. In addition, immobilization itself restricts chain flexibility resulting in an increase in ΔpK_a.

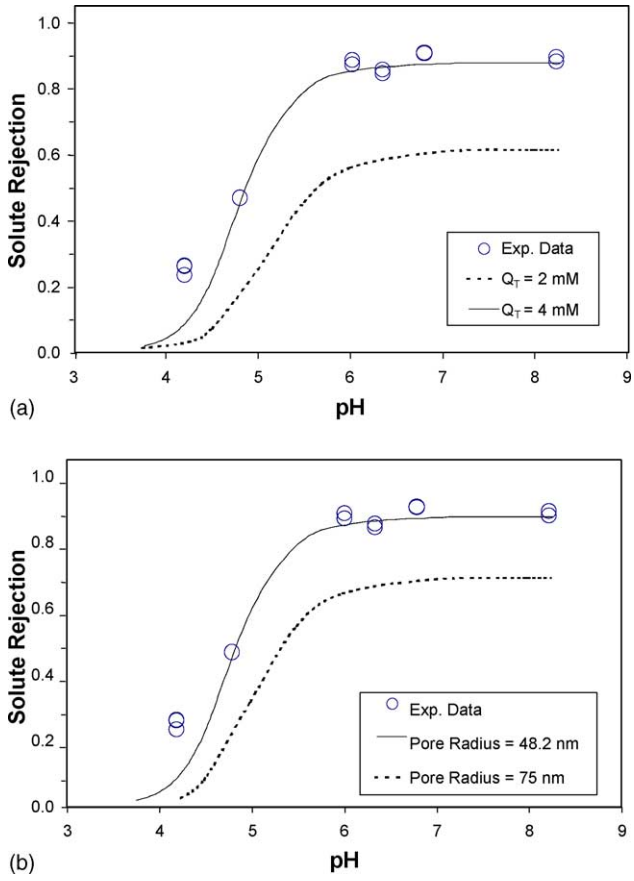

Fig. 13. Dependence of the calculated solute rejection on (a) fixed membrane charge (Q_T) and (b) pore radius for a Na_2SO_4 solution (0.5 mM) using a silica-based microporous membrane functionalized with poly(L-glutamic acid) ($n = 356$) (p$K_a = 5$, $\Delta P = 0.7$ bar).

4.3.2.2. Effect of fixed membrane charge (Q_T) and pore radius (R_p) on solute rejection. The dependence of the calculated solute rejection (0.5 mM Na_2SO_4) on both the overall concentration of fixed ionizable groups (Q_T) and pore radius (R_p) is shown in Fig. 13 ((a) effects of Q_T, (b) effects of R_p). These calculations are based on the PAA region thickness values shown in Fig. 10 for the silica–PE membrane functionalized with PLGA ($n = 356$). An average pK_a of 5 was used for the immobilized polypeptide and the applied transmembrane pressure was 0.7 bar. As shown Fig. 13a, reduction in Q_T by a factor of two results in a significant decrease in retention of dilute divalent solutions (~30% at pH 8). At lower values of Q_T, the effects of ion partitioning are limited (Eq. (6)) and the electric potential established by the attached PAA is reduced resulting in lower ion rejection. Differences in the calculated rejection associated with each value of Q_T become smaller at lower pH because the degree of ionization (see Eq. (1)) of both membranes is approaching zero.

The effect of pore radius on the calculated rejection, depicted in Fig. 13b, provides some insight on the possible significance of pore size distribution. The average

pore radius ($R_{p,ave}$) of the silica-based support used in this study was 48.2 nm with a standard deviation (σ) of approximately 20.5 nm ($\sigma/R_{p,ave} = 0.43$). Using a log-normal density function to characterize the pore size distribution, Saksena and Zydney [36] report that for membranes with $\sigma/R_{p,ave} = 0.5$ approximately 14% of the pores have radii $R_p > 1.5R_{p,ave}$. Model calculations using an average pore radius of 75 nm ($\sim 1.5R_{p,ave}$) showed a solute rejection of approximately 71.4% at pH 8. This value is significantly lower than that predicted for a membrane with an average pore size of 48.2 nm (rejection = 88%) due to reduced PAA pore coverage. These results explain the observed drop in solute retention shown by these functionalized supports at higher permeate flux (see Fig. 8). At higher applied pressure, the flux through these larger pores plays a more prominent role resulting in lower solute rejection.

5. Conclusions

The ultra-low pressure (<1 bar) separation of dilute electrolytes, such as environmentally toxic As(V) and Cr(VI), from aqueous solutions can be achieved in microporous membranes (cellulosic, silica/polyethylene composites) through immobilization of charged poly(amino acids). Ion selectivity was found to depend solely on the acidic (i.e. PLGA) or basic (i.e. PLA and PLL) properties of the attached biomolecule. The measured solute retention was greatly influenced by solute type (i.e. valency, inorganic/organic), ionic strength, solution pH and the loading and pore coverage (degree of polymerization) of the attached polypeptide. Membranes functionalized with PLGA showed pH-sensitive permeability and ion-selectivity. This controlled behavior was attributed to the conformational transitions of PLGA and was not observed for membranes functionalized with PLA or PLL.

The proposed model allows for calculation of ion transport in porous media containing immobilized poly(amino acids) using input parameters of estimated polypeptide pore coverage and surface charge density. Unlike conventional NF theory, parameters associated with the host material (i.e. pore size, thickness) are not used as model parameters. This model accounts for radial variations in electric potential and solute concentration, both inherent properties of charged porous membranes. The dynamic behavior (i.e. pore coverage) of the attached poly(amino acids) can be determined through permeability measurements at varying solution conditions. Thus, changes in the solvent flux due to transitions in the morphology of the grafted macromolecule are taken into consideration. Using these estimates of the brush thickness, the overall fixed membrane charge can be calculated through comparison of the solute rejection (from model) with experimentally measured values. Furthermore, this model allows for evaluation of the average pK_a associated with the attached polypeptide. The estimated pK_a shift of immobilized PLGA corresponds fairly well with solution-phase experiments found in the literature. Although ion transport in grafted porous membranes is much more complex than the behavior described by this idealized approach, these model calculations provide important fundamental insights regarding the proper design of these advanced membrane architectures.

Acknowledgements

The authors recognize the NSF-IGERT program for the partial support of this research work. Thanks are also due to the US EPA STAR Nanotechnology Program for additional funding of this project.

Nomenclature

A	hydraulic permeability ($cm^3/(cm^2\,s\,bar)$)
c_i	concentration of ion i (mol/m^3)
C_i^m	centerline ion concentration in the membrane phase (mol/m^3)
D_i	ion diffusivity (m^2/s)
F	Faraday constant (96487 C/mol)
$[H^+]$	proton concentration in solution (mol/m^3)
J_i	overall ion flux in the pore ($mol/(m^2\,s)$)
$j_{r,i}$	ion flux in the radial direction ($mol/(m^2\,s)$)
$j_{x,i}$	ion flux in the axial direction ($mol/(m^2\,s)$)
J_v	total solvent flux (m/s)
$J_{v,p}$	solvent flux within the membrane pore (m/s)
K_a	dissociation constant (mol/m^3)
K_{a0}	apparent dissociation constant of the corresponding monomer (mol/m^3)
K_i	defined by Eq. (18)
L_i	defined by Eq. (18)
n	number of repeat units associated with an amino acid sequence
P	hydraulic pressure (bar or Pa)
q_w	charge density based on the internal surface of the pore (C/m^2)
Q	fixed charge density based on the internal volume of the pore (mol/m^3)
Q_T	total available ionizable groups based on the pore volume (mol/m^3)
r	radial variable of pore (m)
R	gas constant (J/(mol K))
R_c	position of the radial interface between the core and PAA regions (m)
R_p	pore radius (m)
T	absolute temperature (K)
u	solution velocity (m/s)
x	axial variable of capillary (m)
z_i	valency of ion i
z_x	valency of membrane charge

Greek letters

α	degree of ionization
ε	membrane porosity
ϵ	dielectric permittivity of the electrolyte solution ($\sim 6.93 \times 10^{-10}$ C^2/(J m))
φ	axial electrostatic potential (V)
Φ	total electrostatic potential in pore (V)
κ	Debye–Brinkman permeability coefficient (m^2)
μ	dynamic viscosity (Pa s)
σ	standard deviation
τ	membrane tortuosity
ψ	radial electrostatic potential (V)

Subscripts

c	core region
1	cation
2	anion

Superscripts

B	PAA region
m	membrane phase

References

[1] M. Yoshikawa, A. Shimada, J. Izumi, Novel polymeric membranes having chiral recognition sites converted from tripeptide derivatives, Analyst 126 (2001) 775.

[2] O. Pieroni, A. Fissi, N. Angelini, F. Lenci, Photoresponsive polypeptides, Acc. Chem. Res. 34 (2001) 9.

[3] D. Bhattacharyya, J.A. Hestekin, P. Brushaber, L. Cullen, L.G. Bachas, S.K. Sikdar, J. Membr. Sci. 141 (1998) 121.

[4] S.M.C. Ritchie, L.G. Bachas, T. Olin, S.K. Sikdar, D. Bhattacharyya, Surface modification of silica- and cellulose-based microfiltration membranes with functional polyamino acids for heavy metal sorption, Langmuir 15 (1999) 6346.

[5] J. Hestekin, L.G. Bachas, D. Bhattacharyya, Poly(amino acid)-functionalized cellulosic membranes: metal sorption mechanisms and results, Ind. Eng. Chem. Res. 40 (2001) 2668.

[6] A.M. Hollman, D. Bhattacharyya, Controlled permeability and ion exclusion in microporous membranes functionalized with poly(L-glutamic acid), Langmuir 18 (2002) 5946.

[7] T. Yamaguchi, A. Tominaga, S. Nakao, S. Kimura, Chlorinated organics removal from water by plasma-graft filling polymerized membranes, AIChE J. 42 (1996) 892.

[8] W. Zhang, S. Nilsson, Helix-coil transition of a titrating polyelectrolyte analyzed within the Poisson–Boltzmann cell model. Effect of pH and counterion valency, Macromolecules 26 (1993) 2866.

[9] Y. Huh, T. Inamura, M. Satoh, J. Komiyama, Counterion-specific helix formation of poly(L-glutamic acid) in a crosslinked membrane, Polymer 33 (1992) 3262.

[10] Y. Ito, Y.S. Park, Y. Imanishi, Nanometer-sized channel gating by a self-assembled polypeptide brush, Langmuir 16 (2000) 5376.

[11] S. Hayashi, T. Abe, N. Higashi, M. Niwa, K. Kurihara, Polyelectrolyte brush layers studied by surface forces measurement: dependence on pH and salt concentrations and scaling, Langmuir 18 (2002) 3932.

[12] M. Ullner, C.E. Woodward, Simulations of the titration of linear polyelectrolytes with explicit simple ions: comparisons with screened Coulomb models and experiments, Macromolecules 33 (2000) 7144.

[13] T. Abe, N. Higashi, M. Niwa, K. Kurihara, Density-dependent jump in compressibility of polyelectrolyte brush layers revealed by surface forces measurement, Langmuir 15 (1999) 7725.

[14] R.P. Castro, H.G. Monbouquette, Y. Cohen, Shear-induced permeability changes in a polymer grafted silica membrane, J. Membr. Sci. 79 (2000) 207.

[15] J.M.M. Peeters, J.P. Boom, M.V. Mulder, H. Strathmann, Retention measurements of nanofiltration membranes with electrolyte solutions, J. Membr. Sci. 145 (1998) 199.

[16] K.S. Spiegler, O. Kedem, Thermodynamics of hyperfiltration (reverse osmosis): criteria for efficient membranes, Desalination 1 (1966) 311.

[17] E. Hoffer, O. Kedem, Hyperfiltration in charged membranes: the fixed charge model, Desalination 2 (1967) 25.

[18] W.R. Bowen, J.S. Welfoot, P.M. Williams, Linearized transport model for nanofiltration: development and assessment, AIChE J. 48 (4) (2002) 760.

[19] R.J. Gross, J.F. Osterle, Membrane transport characteristics of ultrafine capillaries, J. Chem. Phys. 49 (1) (1968) 228.

[20] R.F. Probstein, A.A. Sonin, D. Yung, Brackish water salt rejection by porous hyperfiltration membranes, Desalination 13 (1973) 303.

[21] X. Wang, T. Tsuru, S. Nakao, S. Kimura, The electrostatic and steric-hindrance model for the transport of charged solutes through nanofiltration membranes, J. Membr. Sci. 135 (1997) 19.

[22] X. Wang, T. Tsuru, S. Nakao, S. Kimura, Electrolyte transport through nanofiltration membranes by the space-charge model and the comparison with Teorell–Meyer–Sievers model, J. Membr. Sci. 103 (1995) 117.

[23] M. Soltanieh, M. Mousavi, Application of charged membranes in water softening: modeling and experiments in the presence of polyelectrolytes, J. Membr. Sci. 154 (1999) 53.

[24] T. Urase, J. Oh, K. Yamamoto, Effect of pH on rejection of different species of arsenic by nanofiltration, Desalination 117 (1998) 11.

[25] J.D. Ramsey, L. Xia, M.W. Kendig, L. McCreery, Raman spectroscopic analysis of the speciation of dilute chromate solutions, Corros. Sci. 43 (2001) 1557.

[26] Y. Sato, M. Kang, T. Kamei, Y. Magara, Performance of nanofiltration for arsenic removal, Water Res. 36 (2002) 3371.

[27] L. Hagel, Aqueous-size-exclusion chromatography, J. Chromatogr. Library 40 (1988) 119.

[28] E. Nightingale, Phenomenological theory of ion salvation. Effective radii of hydrated ions, J. Am. Chem. Soc. 73 (1959) 1381.

[29] B. Van der Bruggen, C. Vandecasteele, Removal of pollutants from surface water and groundwater by nanofiltration: overview of possible applications in the drinking water industry, Environ. Pollut. 122 (2003) 435.

[30] M. Soltanieh, S. Sahebdelfar, Interaction effects in multicomponent separation by reverse osmosis, J. Membr. Sci. 183 (2001) 15.

[31] T.K. Dey, Ramachandhran, B.M. Misra, Selectivity of anionic species in binary mixed electrolyte systems for nanofiltration membranes, Desalination 127 (2000) 165.

[32] J. Schaep, C. Vandecasteele, A.W. Mohammad, W.R. Bowen, Modelling the retention of ionic components for different nanofiltration membranes, Sep. Purif. Technol. 22–23 (2001) 169.

[33] E.L. Cussler (Ed.), Diffusion Mass Transfer in Fluid Systems, second ed., Cambridge University Press, New York, 1997.

[34] A. Neto, E. Filho, M. Fossey, J. Neto, Polyacids self-dissociation model, J. Phys. Chem. B 101 (1997) 9833.

[35] D. Olander, A. Holtzer, The stability of the polyglutamic acid α helix, J. Am. Chem. Soc. 90 (1968) 4549.

[36] S. Saksena, A.L. Zydney, Pore size distribution effects on electrokinetic phenomena in semipermeable membranes, J. Membr. Sci. 105 (1995) 203.